Parameterization of Blowing-Snow Sublimation in a Macroscale Hydrology Model

L. C. BOWLING*

Department of Civil and Environmental Engineering, University of Washington, Seattle, Washington

J. W. POMEROY+

Institute of Geography and Earth Sciences, University of Wales, Aberystwyth, United Kingdom

D. P. LETTENMAIER

Department of Civil and Environmental Engineering, University of Washington, Seattle, Washington

(Manuscript received 3 November 2003, in final form 19 March 2004)

ABSTRACT

An algorithm that parameterizes the topographically induced subgrid variability in wind speed, snow transport, and blowing-snow sublimation was designed for use within macroscale hydrology models and other large-scale land surface schemes (LSSs). The algorithm is intended to provide consistent estimates of the relative influence of sublimation from blowing snow for continental-scale river basins, while balancing the land surface water and energy budgets. In addition to the standard LSS inputs, the model requires specification of the standard deviation of terrain slope, the mean fetch, and the lag-1 autocorrelation of terrain gradients. Sublimation fluxes are solved for each vegetation class, for each model grid cell. Model results are compared to observed snow water equivalent (SWE) and simulated estimates of sublimation from blowing snow for two small tundra watersheds: Imnavait Creek, Alaska, and Trail Valley Creek, Northwest Territories, Canada, produced by two different small-scale distributed blowing-snow algorithms. The macroscale algorithm reproduced most aspects of the variability between years and between vegetation types predicted by the more detailed models. The macroscale model was subsequently used to estimate sublimation from blowing snow and the snowpack for the 8000-km^2 Kuparuk River watershed in northern Alaska. Annual average sublimation from blowing snow predicted by the model for this region varies from 47 mm in the foothills of the Brooks Range to approximately 31 mm on the Arctic coastal plain; sublimation was primarily controlled by topographic limitations on fetch in the foothills and by precipitation and vapor pressure on the coastal plain.

1. Introduction

The transport of snow by wind is prevalent over tundra, high to midlatitude grasslands, high-altitude steppes, alpine zones, and ice sheets (Berg 1986; Petropavlovskaya and Kalyuzhnyi 1986; Groisman et al. 1997; Mann et al. 2000). Observations of the frequency of occurrence of blowing-snow events range between 16 to 35 days a year in northern Kazahkhstan (Petropavlovskaya and Kalyuzhnyi 1986) to over 90 days a year along the Russian Arctic coastal plain and in the Colorado alpine region (Berg 1986; Groisman et al. 1997). Déry and Yau (1999) estimate that between 10 and 60 blowing-snow events occur per year on the Alaskan North Slope. Blowing-snow events involve erosion, horizontal transport, deposition, and in-transit snow sublimation and play an important role in the spatial and temporal distribution of water and energy fluxes in many high-latitude regions. Tabler (1975a) estimated that over half of wind-transported snowfall sublimates in the high plains of southeastern Wyoming. In the same region, Schmidt (1982) estimated that 39% of transported snow sublimates. Average monthly rates of sublimation calculated for Halley Station, Antarctica, varied between 0.13 to 0.44 mm day^{-1} (King et al. 2001). Pomeroy and Essery (1999) measured maximum sublimation rates during blowing-snow events of 1.2 to 1.8 mm day^{-1} in the Canadian prairies.

Various studies indicate that sublimation during blowing-snow events can represent a significant loss of moisture to the atmosphere over the winter in the tundra, alpine, and interior grasslands (Benson 1982; Berg

* Current affiliation: Department of Agronomy, Purdue University, West Lafayette, Indiana.

+ Current affiliation: Department of Geography, University of Saskatchewan, Saskatoon, Saskatchewan, Canada.

Corresponding author address: Dr. L. C. Bowling, Department of Agronomy, Purdue University, 915 W. State Street, West Lafayette, IN 47907-2054.
E-mail: bowling@purdue.edu

1986; Dyunnin 1959; Schmidt 1972; Pomeroy 1989; Kane et al. 1991; Hinzman et al. 1996; Hood et al. 1998). On the low end, estimates of total seasonal precipitation lost to blowing-snow sublimation are around 15% in the Colorado Front Range where warm temperatures often prevail during winter, limiting the frequency of blowing snow (Hood et al. 1998), and 10% at Halley Station, on an Antarctic ice shelf in highly stable conditions (King et al. 2001). Such estimates increase to 23% to 41% of annual snowfall in the Canadian Prairies and 21% to 34% in arctic Alaska where it appears that entrainment of relatively dry air (lower vapor pressure) sustains sublimation during blowing snow, and cold winters permit a high frequency of events (Pomeroy et al. 1993; Pomeroy and Li 2000; Liston and Sturm 2002). However, the importance of snow sublimation at regional scales is not well established. Direct measurements of sublimation are difficult (Pomeroy and Essery 1999), and water budgets in windswept environments are highly unreliable because of precipitation gauge undercatch, particularly where unshielded gauges are employed (Goodison et al. 1998; Pomeroy and Goodison 1997).

Adequate representation of sublimation is important not only for correct prediction of spring runoff, but also for determination of the spatial distribution of energy and water fluxes in midwinter and their subsequent influence on atmospheric circulation. In the past, macroscale hydrology models have accounted for sublimation from the snowpack, while neglecting the sublimation of blowing snow during transport. Attempts have been made to create less computationally intensive versions of point-scale models for scaling to larger areas (e.g., Bintanja 1998; Déry and Yau 2001; Essery et al. 1999; Liston and Sturm 1998; Pomeroy et al. 1997). However, snow transport, and hence sublimation, in point-scale models is sensitive to the path length, or fetch, over which the atmospheric boundary layer develops (Pomeroy et al. 1993; Pomeroy and Li 2000). Calculations of blowing-snow fluxes over areas with varying fetch have used spatially distributed wind fields over gridded domains such that the fetch is calculated for each model grid cell (Essery et al. 1999; Liston and Sturm 1998). Alternatively, the mean fetch has been calculated for various landscape elements in a region as a preprocessing step (Pomeroy et al. 1997). The effect of the variation in fetch across the domain of a macroscale model grid cell (typically ⅛°–2° latitude by longitude) on sublimation rates is an issue that remains to be quantified. In addition, the total sublimation rate during blowing-snow events has a highly nonlinear dependence on wind speed (Essery et al. 1999; King et al. 2001; Mikhel and Rudneva 1967), and hence to topography (van den Broeke et al. 1999).

There is some debate in the literature as to whether blowing-snow models tend to overpredict latent heat fluxes when negative thermodynamic feedbacks in the near-surface boundary layer are neglected (Déry et al. 1998; Déry and Yau 2001; Xiao et al. 2000; Pomeroy and Li 2000). Based on work in Antarctica, Mann et al. (2000) and King et al. (2001) observed strong vapor pressure feedbacks following the initiation of blowing snow resulting in saturation of the air. Observations of saturation in the boundary layer during high wind speeds have not been widespread outside Antarctica (e.g., Schmidt 1982; Pomeroy and Li 2000). Pomeroy and Li (2000) demonstrated that simulations of thermodynamic feedback due solely to blowing-snow sublimation do not reproduce temperature and humidity profiles observed during blowing-snow events. They argue that the observed records of humidity and temperature implicitly account for the large-scale advection and entrainment that should minimize saturation of the near-surface layer in the natural system. Recent concerns regarding overmeasurement of humidity by Vaisala hygrothermometers also suggest that the case for humidity feedbacks may be overstated (Déry and Stieglitz 2002). In addition, simulations accounting for entrainment have been shown to at least partially overcome the thermodynamic suppression of sublimation (Bintanja 2001; Déry and Yau 2001).

This paper describes an algorithm that parameterizes the topographically induced subgrid variability in wind speed, snow transport, and sublimation for use within a macroscale hydrology model. Sublimation fluxes are solved for multiple vegetation classes within each model grid cell. Model predictions are compared with observed end-of-season snow water equivalent (SWE) and simulated sublimation from blowing snow for three tundra sites in North America, shown in Fig. 1.

2. Model description

The Variable Infiltration Capacity (VIC) model is a macroscale hydrology model that represents subgrid variability in infiltration capacity and related ''fast'' runoff response to precipitation through a variable infiltration curve (Liang et al. 1994) and ''slow'' runoff response via a nonlinear relationship between baseflow and deep soil moisture. It includes a mosaic-type vegetation scheme to represent multiple vegetation types within each grid cell, multiple soil layers, and subgrid representation of elevation zones in areas of complex topography. VIC has been applied in many diverse environments, including a global application at 2° latitude/longitude resolution (Nijssen et al. 2001) and across the contiguous United States at ⅛° resolution (Maurer et al. 2002). Recent work has focused on making the model more representative of northern regions, including representation of frozen soils, spatial variability in snow and frost, and lakes and wetlands (Cherkauer and Lettenmaier 1999; Cherkauer et al. 2003).

The blowing-snow algorithm described in this paper is designed to work within the structure of the existing VIC mass and energy-balance snow model, which describes the temporal variation of snow water equivalent and snow surface temperature within a model grid cell

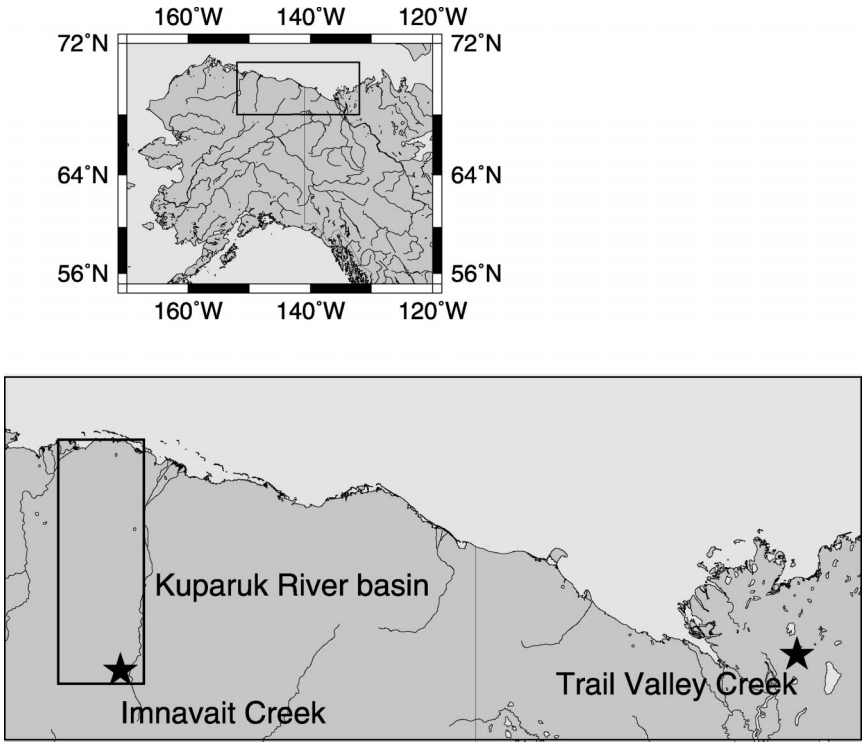

FIG. 1. Location map of the three study areas used to evaluate the blowing-snow algorithm.

(Cherkauer and Lettenmaier 1999; Cherkauer et al. 2003). Ground snow accumulation, sublimation, and melt are simulated using a two-layer surface energy-balance model. Precipitation occurring below a threshold temperature is assumed to be snow. The model accounts for the energy advected by rain, throughfall, or drip (when overstory is present), as well as net radiation, ground heat flux, and sensible and latent heat. Incoming short- and longwave radiation and wind speed are attenuated through the canopy, if present. If snow is present, it is assumed to cover the understory for purposes of radiation transfer. For each vegetation fraction within the grid cell, the time rate of change of snow water (W_e) is

$$\frac{dW_e}{dt} = P - M - p \times Q_v - Q_e, \tag{1}$$

where dW_e/dt is the rate of snow water accumulation, P is precipitation, M is snowmelt and drainage, Q_v is the sublimation from blowing snow, and Q_e is evaporation and sublimation from the snowpack, for a time increment dt. All of the terms are in units of millimeters per time step. The spatial probability of occurrence of blowing snow, p, is unitless. To aggregate the fluxes from each landscape element to grid-scale values, the fluxes are weighted by the respective area of the landscape element. Traditionally, the mass balance equation (1) would include a divergence term to represent the downwind transport of saltating and suspended snow out of (into) each landscape element. It is assumed that at the scale of application of the VIC model, transport of blowing snow between vegetation elements is negligible relative to the rate of snow sublimation in transit within a vegetation element. The consequences of this assumption are further discussed below.

The method of calculating sublimation from blowing snow is a derivative of existing column and small-scale spatially distributed blowing-snow models (e.g., Essery et al. 1999; Pomeroy et al. 1993; Pomeroy and Li 2000; Liston and Sturm 1998). The model structure, shown in Fig. 2, is summarized below. The mass transport of blowing snow for fully developed flow, $Q_{t\_\max}$, (kilograms per meter per second), is dependent on the mass concentration of saltating and suspended particles, as follows:

$$Q_{t\_\max} = \phi_r u_r h_* + \int_{h_*}^{z_t} \phi_s(z) u(z)\, dz, \tag{2}$$

where $u(z)$ is the height-dependent wind speed (meters per second), assumed to follow a logarithmic profile; ϕ_r and u_r are the mass concentration (kilograms per meters cubed) and particle speed (meters per second) in the saltating layer, assumed constant with height, z (meters); and ϕ_s is the vertical profile of mass concentration in the suspended layer (kilograms per meters cubed). The particle speed, u_r (meters per second), is estimated as 2.8 times the threshold shear velocity (Pomeroy et al. 1993). The threshold shear velocity is calculated from air temperature (Li and Pomeroy 1997).

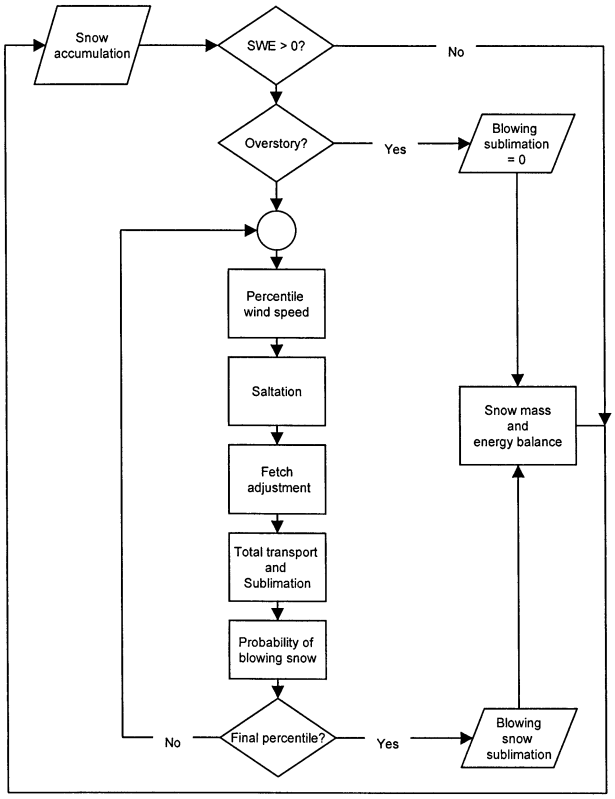

FIG. 2. Schematic illustrating the calculation of sublimation from blowing snow and interaction with the existing VIC snow model.

The height of the saltating layer, h_* (meters), is estimated from wind shear (Pomeroy and Male 1992). The height of the suspension layer, z_t (meters), is found as the height at which ϕ_s reaches zero (Liston and Sturm 1998). The mass concentration of suspended transport is calculated according to the power-law relationship of Kind (1992), based on height and surface shear stress.

The maximum sublimation rate, Q_v (millimeters per time step), is based on the sublimation loss rate of the saltating and suspended particles, as follows:

$$Q_v = \left(\frac{1000\Delta t}{\rho_w}\right)\left[(\Psi_r \phi_r h_*) + \int_{h_*}^{z_t} \Psi_s(z)\phi_s(z)\, dz\right]. \quad (3)$$

Here, Ψ_r and Ψ_s are the sublimation-loss rates of particles in the saltating and suspended layers (per second), respectively, equal to the time rate of change of the particle mass, normalized by the particle mass. The first term is a conversion factor that results in units of millimeters per time step for use in Eq. (1), where Δt is the number of seconds per time step, and ρ_w is the density of water (kilograms per meters cubed). The mean particle mass is found by assuming that particle radii follow a two-parameter gamma probability density function, based on the work of Schmidt (1982) and Pomeroy (1989). The time rate of change of particle mass is calculated according the formulation of Thorpe and Mason (1966) and is proportional to the undersaturation of atmospheric water vapor with respect to ice, defined as the fractional atmospheric relative humidity minus one. The increase in undersaturation with height is represented using a log-normal relationship in the manner of Pomeroy and Li (2000). The blowing-snow algorithm occasionally predicts sublimation rates that cannot be met by the available vertical energy, as subgrid advection of energy is not considered, leading to model instabilities. To avoid this problem, the maximum areal sublimation rate in the model is capped at 0.1 mm h^{-1}, based on the maximum rates of 0.05–0.075 mm h^{-1} observed using an eddy correlation system in moderate prairie blowing-snow storms by Pomeroy and Essery (1999).

The probability of blowing-snow occurrence over a uniform spatial area (i.e., fractional area experiencing snow transport for each time step) is calculated using a normal probability distribution dependent on wind speed, snow age, exposed vegetation roughness, and air temperature (Li and Pomeroy 1997; Pomeroy and Li 2000). By this method, the effect of the meteorological history of the snowpack on threshold conditions for transport are included, and the occurrence of blowing-snow sublimation is restricted when vegetation height is high relative to the snow depth. It is therefore not necessary to suppress all transport when the snow depth is less than an assigned vegetation snow-holding capacity, in the manner of Liston and Sturm (1998).

For inclusion in the VIC model, the blowing-snow algorithm must be applicable for grid-cell resolutions on the order of ½° latitude by longitude (approximately 1000 to 2200 km^2 in area within the circumpolar Arctic domain). In order to represent the large wind speed variations in regions of complex terrain, the spatial distribution of wind speed within the model grid cell is represented by a Laplace distribution (Essery 2001). Parameters of the distribution are calculated from the distribution of terrain slopes within the grid cell at an effective spatial resolution of 50 m, as described below. For large spatial domains, the parameters of the slope distribution are calculated at 30 arc second resolution (400 to 900 m) and rescaled to be representative of the 50-m distribution using simple (monofractal) scaling relationships. The actual transport capacity of the boundary layer—that is, the mass flux of snow particles that can be carried through saltation and suspension—depends upon distance along a homogeneous fetch.

a. Subgrid variability in wind speed

Based on the linear theory of wind flow over topography, Essery (2001) demonstrated that the probability distribution of wind speed must be the same as the probability distribution of terrain gradients. The Laplace (double exponential) probability distribution approximates the empirical distribution of terrain gradients for two tundra catchments in North America with very different topographies: Imnavait Creek, Alaska (calculated

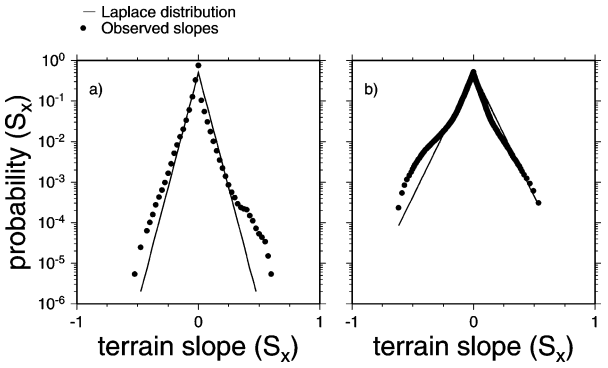

FIG. 3. Laplace distribution fit to east–west terrain slopes for (a) Trail Valley Creek and (b) Imnavait Creek.

at 50-m resolution), and Trail Valley Creek, Northwest Terrifories, Canada (calculated at 40-m resolution), as shown in Figs. 3 and 4. The Laplace distribution offers an advantage over other probability distributions because it is specified by only two parameters and is easily integrated.

Using a Laplace distribution, the probability distribution function of wind speed within a model grid cell is

$$p(w) = \frac{1}{2\sigma_w} \exp\left(-\frac{|w - u_o|}{\sigma_w}\right), \tag{4}$$

where w (meters per second) is the wind speed, σ_w (meters per second) is the standard deviation of wind speed, and u_o (meters per second) is the grid-cell mean (and median) wind speed. We assume that u_o is represented by the wind speed estimated using least-distance-squared interpolation from station observations to the grid-cell centers. In general, meteorological towers for station observations are frequently located on flat fetches; therefore, the interpolated observations may be different than the true mean.

As derived by Essery (2001), σ_w is a function of u_o, the standard deviation of terrain gradient (σ_t) and the Fourier transform of the terrain gradient autocorrelation function. The terrain gradient autocorrelation is a measure of the extent to which the terrain gradient at distance x is related to the gradient at distance $x + n\Delta x$ for $n = 1, 2, \ldots$, calculated as follows:

$$\rho(n) = \frac{\langle s(x)s(x + n\Delta x)\rangle}{\langle s^2\rangle}, \tag{5}$$

where s is the terrain gradient, and $\langle\ \rangle$ denotes a spatial average. Lag one referes to the value of the autocorrelation function for $n = 1$.

In order to investigate wind speed variation (as predicted by a linear wind-flow model) with respect to topographies with a range of values in autocorrelation, Essery (2001) generated synthetic topographies of a specified autocorrelation. He found that the function describing σ_w is nearly linear for synthetic topographies with lag-one autocorrelation values between 0.0 and 0.9. To avoid computationally intensive numerical integrations, the wind speed standard deviation is therefore estimated based on the Essery (2001) data as

$$\sigma_w = u_o\sigma_t(2.44 - 0.43\phi), \tag{6}$$

where ϕ is the lag-one gradient autocorrelation. For example, for the Trail Valley Creek watershed, Essery et al. (1999) computed $\phi = 0.81$, and $\sigma_t = 0.044$, which yields a wind speed coefficient of variation, $\sigma_w/u_o = 0.09$. That is, the wind speed spatial variation is low with respect to the mean.

The VIC wind parameterization requires the standard deviation of terrain gradients and the lag-one gradient autocorrelation for each vegetation type, and wind direction for each model grid cell. For simplicity, we compute the standard deviation for the eight primary wind directions and then average to yield an effective value that varies with vegetation type. For limited testing in Alaska and the Northwest Territories the standard deviation of terrain gradients varied only slightly based on wind direction. In regions where this is not the case,

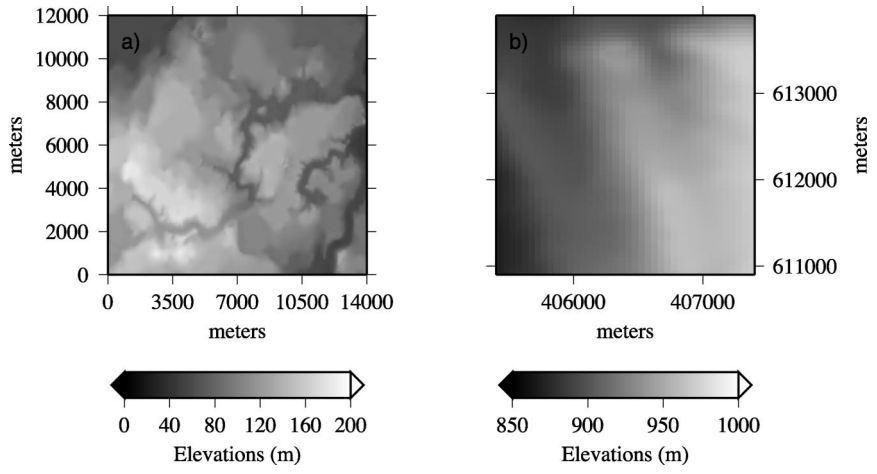

FIG. 4. Digital elevation models of (a) Trail Valley Creek and (b) Imnavait Creek.

simple averaging has the potential to result in larger errors than when averaging the results of the sublimation calculation for each wind direction (because of the highly nonlinear dependence of sublimation on wind speed).

The total sublimation flux due to the spatially variable wind field is solved by summing the sublimation calculated for the average wind speed of 10 equally probable intervals:

$$Q_v = \sum_{i=1}^{n} p_i Q_{vi}(u_i) \quad \text{and}$$

$$u_i = E[w] = \frac{\int_{Z_i}^{Z_{i+1}} p(w) w \, dw}{\int_{Z_i}^{Z_{i+1}} p(w) \, dw} = \frac{\int_{Z_i}^{Z_{i+1}} \frac{1}{2}\frac{w}{\sigma_w} \exp\left(-\frac{|w - u_o|}{\sigma_w}\right) dw}{\int_{Z_i}^{Z_{i+1}} \frac{1}{2}\frac{1}{\sigma_w} \exp\left(-\frac{|w - u_o|}{\sigma_w}\right) dw}, \tag{7}$$

where Q_{vi} is the sublimation rate for each wind speed u_i, n is the number of probability intervals to be solved, and p_i (here equal to $1/n$) is the probability that the spatially varying wind speed falls within probability class i; z_{i+1} is the deviate of the upper boundary of the ith probability class. The wind speed, u_i, is the expected value of the wind probability density function [Eq. (4)] between limits calculated from p_i, as follows:

$$z_0 = -\infty,$$

$$z_{i+1} = u_o + \sigma_w \ln\left[\exp\left(\frac{z_i - u_o}{\sigma_w}\right) + 2p_i\right], \quad \text{for } z_{i+1} \le u_o,$$

$$z_{i+1} = u_o - \sigma_w \ln\left[\exp\left(-\frac{z_i - u_o}{\sigma_w}\right) - 2p_i\right], \quad \text{for } z_{i+1} > u_o$$

$$z_n = \infty. \tag{8}$$

b. Upscaling to large spatial domains

Application of the blowing-snow algorithm to large spatial domains is complicated by the absence of digital elevation data at resolutions sufficient to derive the terrain gradient distributions. The distribution of terrain slopes at 50-m resolution must therefore be derived from the global topography at 30 arc seconds (GTOPO30) resolution digital elevation data, which are available globally.

Several researchers have investigated the monofractal nature of topography (Klinkenberg and Goodchild 1992; Xu et al. 1993; Zhang et al. 1999) as well as its multifractal characteristics (Lavalée et al. 1993; Lovejoy et al. 1995). The convenience of monofractal topography is that it implies simple scaling. That is, for rescaled topography Z_l,

$$Z_l(x) = Z(lx), \tag{9}$$

a scaling function exists such that

$$E[Z_l^h] = l^{h\theta} E[Z_l^h] \tag{10}$$

for all moments of order h, where θ is the scaling constant, equal to 2 minus the fractal dimension, D, for a surface (Kono 1985).

Lovejoy et al. (1995) demonstrated that the topography of Deadman's Butte, Wyoming, is multifractal in nature, which therefore requires a multiscaling approach when transforming between resolutions. For both simple and multiscaling processes, the statistical moments, $m(h)$, should be linear with respect to the scale, l, in log–log space. A random field, Z, is considered wide-sense multiscaling if the slopes of these linear functions, $S(h)$, are nonlinear with respect to h (Gupta and Waymire 1990). The Upper Kuparuk River basin is a tributary to the Kuparuk River located in the foothills of the Brooks Range, Alaska, adjacent to the Imnavait Creek watershed (see Fig. 1). A 50-m-resolution digital elevation model (DEM) is available for the Upper Kuparuk River basin (Walker 1996), allowing for the sampling of statistical moments of the terrain gradients, shown in Fig. 5a, with respect to $\log(l)$. As indicated by the black dots, the moments are nearly linear with respect to l for several grid resolutions (50, 100, 200, 400, 800, and 1600 m), calculated from the 50-m DEM. The corresponding GTOPO30 DEM was transformed to the universal transverse mercator (UTM) projection at 800-m resolution (grid-cell distances in the geographic projection vary between 600 and 900 m at this latitude). The moments for this DEM (shown by open diamonds in Fig. 5a) for resolutions of 800 and 1600 m indicate good correspondence between the 50- and 800-m DEMs. At resolutions above 1600 m, the moments become increasingly nonlinear for both DEMs. Lovejoy et al. (1995) noticed the same nonlinearity for coarse-resolution grids and attributed it to the small sample size at these resolutions. The linear best-fit lines for the 50-m DEM are therefore calculated from the first six values of l for each moment. Unfortunately, with only two points available from the 800-m DEM, it is not possible to recover the same slopes from the 800- and 50-m DEMs, as indicated in Fig. 5b. The empirically derived lines in Fig. 5b are convex downward with respect to the straight line expected from simple scaling, indicating that the multiscaling model is more appropriate for this terrain. However, the difference is small for moments up to two (the variance), so we conclude that simple scaling is appropriate for recovering the variance at 50-m resolution from the 800-m DEM.

Because the slopes of the moments cannot be recov-

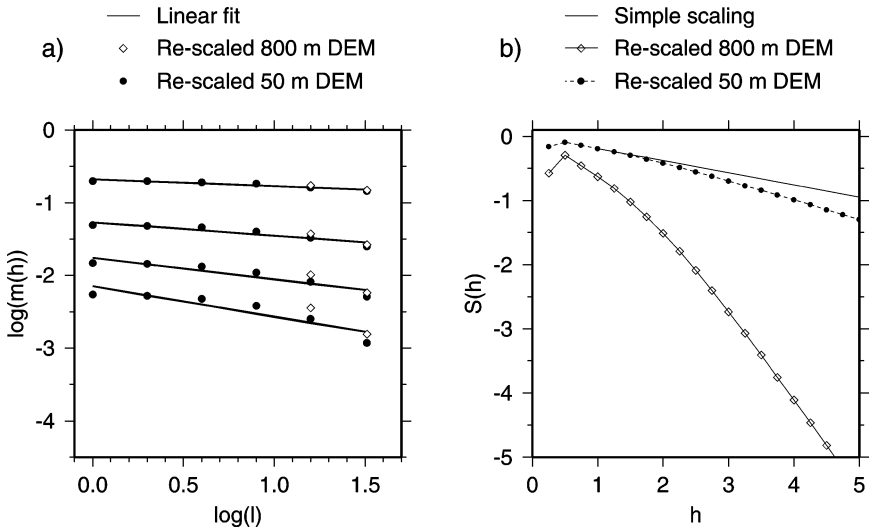

FIG. 5. Procedure for estimating terrain parameters from coarse-resolution DEMs using data from the Kuparuk River basin: (a) the log of the moments, $m(h)$, of the distribution of terrain slopes vs the log of the scale, 1. The moment order is from top to bottom: $h = 0.5$, 1.0, 1.5, and 2.0. (b) The slopes, $S(h)$, of the fitted lines in (a) vs the moment order, h. The solid black line indicates the relationship expected from simple scaling.

ered from the 800-m DEM, an alternative method is used to calculate the fractal dimension of the surface, and therefore the scaling constant, θ. The surface fractal dimension for the region spanned by one model grid cell is calculated using the variogram technique as described by Xu et al. (1993), including all elevation pairs from the GTOPO30 DEM within a VIC model grid cell. This involves plotting the log of the average elevation difference of all pairs separated by an incremental distance. The fractal dimension is calculated as the slope of the first linear portion of this graph. For the Upper Kuparuk data, this yields an estimate of the fractal dimension of 2.18, so $\theta = 2 - D = -0.18$. For comparison, the estimate of θ taken from the 50-m data in Fig. 5b is $\theta = [dS(h)]/dh|_{h=1} = -0.19$.

To determine the standard deviation of the distribution of terrain slopes for each VIC model grid cell, the variance of the terrain slope is first calculated for each VIC model grid cell. The GTOPO30 variance is rescaled according to Eq. (10), where θ is calculated from the fractal dimension of the corresponding VIC grid cell estimated using the variogram method. The scale, l, is equal to 16 (800 m/50 m), and the moment, h, equals 2, corresponding to the variance. Using this approach for the Upper Kuparuk basin, the estimate of the standard deviation of terrain gradients from the 30 arc second DEM (0.048 m/m), is rescaled to 0.079 m/m. This is within 6.8% of the original estimate from the 50-m DEM (0.074 m/m).

c. Nonequilibrium transport

The total mass of downwind transport and sublimation of blowing snow depends upon the length of downwind development of the boundary layer, or fetch, from a point where blowing-snow transport does not occur (Pomeroy et al. 1993). The observations of Takeuchi (1980) and modeling by Pomeroy et al. (1993) indicate that the increasing downwind transport of snow over a region of homogeneous vegetation and wind speed a distance, x (meters), from the initiation of transport follows an exponential profile of the form

$$Q_t(x) = Q_{t\max}[1 - \exp(-\mu x/f_{\max})], \qquad (11)$$

where $Q_{t\max}$ is the maximum rate of transport for fully developed flow given in Eq. (2) (kg m^{-1} s^{-1}), $f_{\max}$ is the fetch length for fully developed flow (meters), and μ is a unitless scaling factor. The scaling factor is fixed at 3.0 following Liston and Sturm (1998) and Essery et al. (1999), a value that provided simulations of snowdrift location that matched observations in their modeling studies.

For any parcel of the grid cell defined by homogeneous vegetation and wind speed, the average transport rate will be the integral of Eq. (11). Since the transport rate is zero by definition at the edge of each of these parcels, the lower boundary of the integration is zero. The upper limit of integration is the average downwind distance for each parcel. The challenge lies in defining this distance as an effective average to be used at large scale.

In arctic tundra landscapes, breaks in fetch are most often related to terrain features such as river incisions, escarpments and divergence in slope and aspect, or vegetation features that serve to inhibit blowing-snow transport (Pomeroy et al. 1997). Man-made features such as roads, pipelines, and snow fences may also be important locally, although they have minimal extent. The control of fetch by either topography or vegetation will change

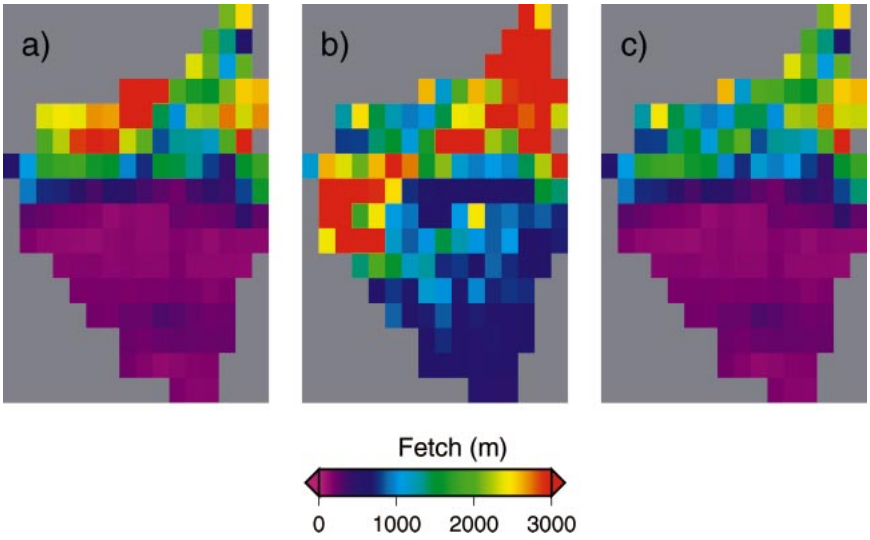

FIG. 6. Comparison of average-grid-cell fetch for the Kuparuk River basin calculated by three methods: (a) based on vegetation type, (b) based on the magnitude of terrain slope, and (c) combined estimate using the minimum fetch estimated from terrain or vegetation.

depending on which factor limits the fetch length. For example, in regions of moderate terrain with varied vegetation cover, fetch is most often controlled by changes in vegetation (Pomeroy and Gray 1995). In regions with reduced vegetation height, such as the high Arctic, topography controls fetch.

Muller et al. (1999) developed a 50-m resolution land cover classification for the Kuparuk River basin in northern Alaska based on Landsat imagery. The eight vegetation classes in the Muller et al. (1999) dataset were regrouped into three dominant classes:

1) dry tundra and barrens, shadows, and low-shrub tundra—primarily found on exposed ridges in the foothills and gravel river beds and roads on the coastal plain;
2) moist prostrate-shrub tundra, wet tundra, open water, and clouds and ice—primarily found on the coastal plain and in valley bottoms; and
3) moist dwarf shrub tussock tundra—primarily found on hill slopes.

Pixels classified as open water are primarily due to the numerous small thaw ponds that predominate on the coastal plain. During the winter, these freeze early and are rapidly indistinguishable from the surrounding vegetation in terms of blowing-snow transport. Pixels classified as clouds or ice represent less than 1.6% of the classified area and have negligible effect on the calculated fetch.

For each VIC model grid cell, the average fetch of each land class was found automatically, using the following algorithm:

- The 50-m vegetation grid corresponding to each ⅛° VIC model grid cell is sampled for each of the four primary wind directions: N–S, E–W, NE–SW, and NW–SE.
- For each 50-m vegetation grid cell, the distance in each direction within the same land class is calculated.
- The four direction values are averaged to obtain the average fetch for all directions for each 50-m cell.
- This fetch is then averaged over all 50-m vegetation grid cells in the same class to obtain an average fetch for each land class.
- Finally, the fetch is averaged over all vegetation classes, to obtain the average fetch for each VIC model grid cell.

The final average fetch for each VIC model grid cell calculated by this method is shown in Fig. 6a. The pattern generally corresponds to expectations, with fetch lengths less than 500 m in the foothills, and between 1000 to 3000 m on the coastal plain.

Calculation of breaks in fetch due to topographic features is complicated by both the resolution of the DEM and identification of the topographic classes that correspond to breaks in fetch. Tabler (1975b) predicted profiles of snowdrifts based on topographic slope along a transect. Consistent with this approach, grid cells were assigned to different topographic classes based on a difference of 0.5% slope, and the average fetch was calculated as described above (shown in Fig. 6b). The topographic classes yield a spatial pattern consistent with the vegetation, although with generally longer fetches.

Figure 6c shows a combined measure of fetch for the Kuparuk River basin calculated as the minimum of either the vegetation-based or the topography-based estimate of fetch. This figure indicates that for much of the basin, the vegetation fetch length is shorter than that calculated from topographic slope. This may indicate

that fetch is predominantly controlled by vegetation throughout the Kuparuk River basin, although the vegetation dataset is of finer resolution and presumably higher quality than the terrain data. In addition, since the vegetation classes are closely correlated with terrain, the short fetch lengths calculated from the vegetation dataset may reflect the evolution of vegetation patterns in response to terrain-induced conditions of snow depth, soil moisture, summer thaw depth, etc. The measure of fetch obtained from topography contains a region of high fetch in the western part of the basin, with a contrasting region of low fetch to the north and east of the higher fetch zone. The vegetation measure shows the reverse signal. The low fetch region in Fig. 6b corresponds to a region of complex terrain (the White Hills) and may indicate fetch limitation by topography that is not reflected in the uniform vegetation coverage.

3. Test applications

a. Imnavait Creek, Alaska

Imnavait Creek is a 2.2-km^2 catchment located in the foothills of the Brooks Range in northern Alaska. Low-growing grasses and sedges are the dominant forms of vegetation, with taller willow shrubs occurring in valley bottoms. Shallow soils and exposed rock are present on the ridges (Liston and Sturm 1998). The topography of Imnavait Creek (shown in Fig. 4b) is gently rolling, with north–south trending ridges spaced approximately 1–2 km apart.

The catchment was represented by one VIC model grid cell with the five vegetation types identified in Liston and Sturm (1998): dry, moist, and wet tundras, shrubland, and bare ground. The simulation was conducted continuously from August 1986 through October 1994, using a 1-h model time step. The terrain distribution and autocorrelation were calculated from a 50-m DEM of the area, so no fractal scaling was needed for this application. Hourly observations of wind speed, relative humidity, and air temperature for the VIC application were obtained from two meteorological towers operated in the basin by the Water and Environment Research Center (WERC), University of Alaska, Fairbanks (UAF) (Kane and Hinzman 2003). Atmospheric pressure is fixed at 95.5 kPa. The remaining meteorological fields necessary to drive the VIC model, incoming longwave and shortwave radiation, are estimated internally to the model, as described by Nijssen et al. (2001).

Observations of relative humidity pose a particular problem in cold regions. At temperatures less than 0°C, saturation vapor pressure (e_s) can be in equilibrium with a surface of either liquid water or ice. It is not always clear how relative humidity (equal to vapor pressure, e_a, over e_s) is measured, although it is frequently measured with respect to liquid water. It is usually assumed that the value with respect to ice is required for sublimation calculations. Humidity measured over water is less than that over ice, so fractional humidity collected with respect to water will reach saturation at values less than 1 [equivalent to e_s(ice)/e_s(water)]. The humidity data from Imnavait Creek do not appear to be limited by this ratio, so no adjustment was performed to the observed data. The quality of the humidity data is questionable below approximately −30°C, but this should have little impact on the calculation of blowing snow as sublimation is restricted because of the low vapor pressure values at extreme cold temperatures.

Daily precipitation was obtained from a Wyoming snow gauge operated at Imnavait Creek. The record was corrected for undercatch of snow and mixed precipitation by first applying a correction for the Wyoming shielded gauge relative to a double-fenced reference gauge (DFIR) (Yang et al. 2000). The ''DFIR precipitation'' was then adjusted to ''true'' precipitation following World Meteorological Organization (WMO) procedures (Goodison et al. 1998). The corrections resulted in an average increase in winter precipitation of 14%.

Time series of basin-averaged SWE and cumulative sublimation simulated by the VIC model with and without the blowing-snow sublimation algorithm are shown in Fig. 7 and summarized in Table 1. Observed SWE averaged over a basin transect is also shown in Fig. 7 (Kane et al. 2000; Kane and Hinzman 2003). Figure 7a illustrates the relative influence of estimated sublimation in this environment; no direct observations of sublimation are available for comparison. Simulated seasonal sublimation from blowing snow (calculated from 1 September through 30 April) varies between 10 and 45 mm for the 7-yr period (1987 through 1994). Vapor flux from the snowpack results in net condensation for six of the seven years, with an average value of 5.7 mm.

Sublimation and redistribution of snow by wind was simulated for the Imnavait Creek watershed for the period September 1985 through May 1990 by Liston and Sturm (1998) using the SnowTran-3D distributed snow-transport model. Wind speeds in the model were resolved for each 20-m pixel via an empirical wind weighting scheme based on terrain slope and curvature. The transport of snow from cell to cell in the direction of the wind, sublimation, erosion, and deposition are calculated in each time step. SnowTran-3D, therefore, explicitly represents the small-scale wind speed variations and fetch that are parameterized in the VIC algorithm; however, it has not been extensively evaluated with respect to observations. Comparison of VIC model results with the distributed model results therefore allows assessment of the ability of the VIC algorithm to parameterize subgrid variability in wind speed and fetch, but provides only a qualitative evaluation of the magnitude of the sublimation fluxes. A daily time step was used for the simulation by Liston and Sturm (1998) and may have introduced errors to the simulation as the blowing-snow model physics are based on subhourly relationships between wind speed and transport (Pomeroy and Gray 1990; Pomeroy et al. 1993).

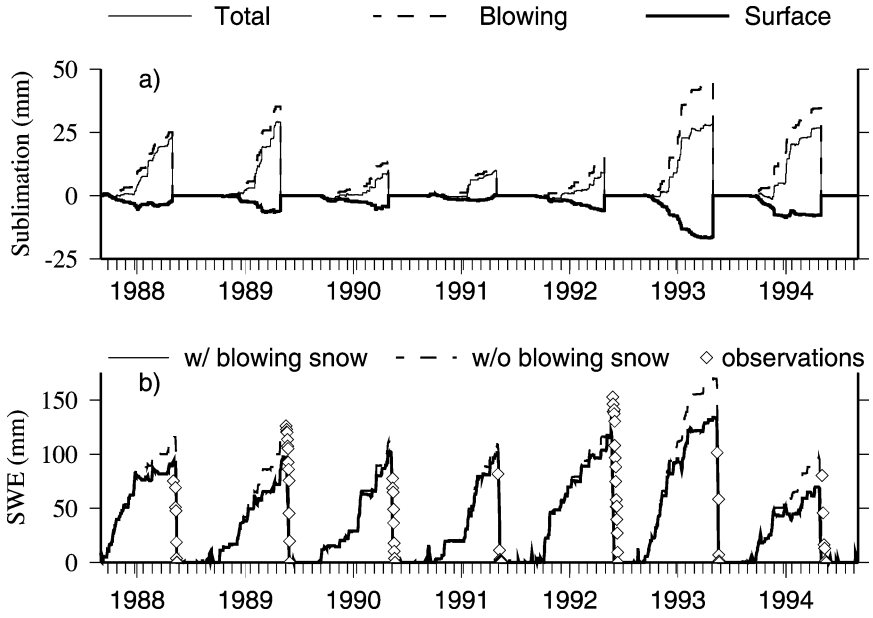

FIG. 7. (a) Cumulative (1 Sep through 30 Apr) blowing-snow, surface, and total sublimation for Imnavait Creek predicted using the VIC model with the blowing-snow algorithm, and (b) basin-average snow water equivalent for Imnavait Creek predicted using the VIC algorithm with and without the blowing-snow algorithm.

VIC model-simulated maximum SWE is shown with the observed maximum SWE from Table 1 for all seven seasons (1987/88 through 1993/94) in Fig. 8a. SWE simulated without the blowing-snow algorithm is also shown. The figure indicates that the VIC algorithm reproduces the observed SWE well for five of the seven years, although on average, VIC underpredicts SWE. This appears to be due to an underestimation of precipitation. As shown in Fig. 8b and Table 1, the accumulated, corrected snowfall that was used in the VIC model is less than the observed SWE in 1989 and 1992. If these two years are neglected from the analysis, on average the annual maximum SWE predicted by the VIC algorithm with blowing snow (101 m) is closer to the observed average (94 mm) than is the VIC prediction without sublimation from blowing snow (121 mm).

Averaged over four WMO Solid Precipitation Intercomparison sites, Yang et al. (2000) found that the Wyoming snow gauge captured 91% of the precipitation measured by a double-fenced reference gauge (9% un-

TABLE 1. Estimated precipitation, SWE, and sublimation for Imnavait Creek, AK.

Year	Precipitation[a]	Observed max SWE[b]	Simulated max SWE[c]		L&S blowing sublimation[d]	Simulated blowing sublimation[e]
			With blowing	Without blowing		
1988	119 mm	78 mm	95 mm	116 mm	25	25
1989	138	155	97	126	38	35
1990	110	106	102	114	13	15
1991	120	82	102	109	NA	10
1992	126	181	122	135	NA	15
1993	166	125	134	170	NA	45
1994	114	80	70	97	NA	35
Average	128 (126)[f]	114 (94)[f]	103 (101)[f]	124 (121)[f]	25[g]	25[g]

[a] Catch corrected. Accumulated from 1 Sep to 30 Apr each year for hours with air temperature $<0°C$, assuming daily precipitation equally distributed over 24 h.
[b] Average SWE observed at numerous locations around the basin in late spring of each year before melt begins. It represents an estimate of the annual maximum (Kane et al. 2000).
[c] Domain average simulated maximum SWE.
[d] From Liston and Sturm (1998).
[e] Accumulated from 1 Sep to 30 Apr, for comparison with Liston and Sturm (1998).
[f] Value in parentheses represents average without data from 1989 and 1992, when the observed precipitation is not enough to account for the observed SWE.
[g] Average from 1988 to 1990.

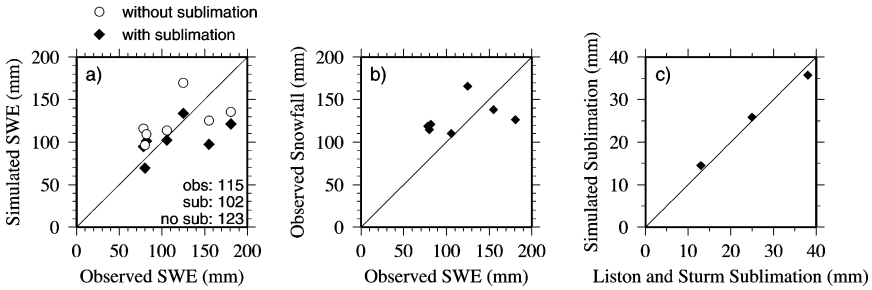

FIG. 8. Comparison of basin-average quantities for Imnavait Creek (a) annual maximum snow water equivalent predicted by the VIC model vs observed maximum snow water equivalent, (b) accumulated (1 Sep through 30 Apr) catch-corrected snow precipitation vs observed maximum snow water equivalent, and (c) accumulated (1 Sep through 30 Apr) blowing-snow sublimation predicted by the VIC model vs sublimation predicted by Liston and Sturm (1998).

dercatch), with an average undercatch of 6% for snowfall and 55% for blowing-snow conditions. Using sublimation estimates from Liston and Sturm (1998), Yang et al. (2000) estimated that the undercatch at Imnavait Creek averaged 32% for 1987, 1988, and 1990. Similarly, Liston and Sturm (2002) estimated 30% undercatch at Imnavait Creek for 1995, 1996, and 1997, again based on simulated sublimation. The corrections applied for this application indicate an average undercatch of 12% at Imnavait Creek. It therefore appears likely that in some years, such as 1989 and 1992, gauge undercatch is a cause of underpredicted SWE.

Liston and Sturm (1998) used an iterative data assimilation approach to estimate total snow precipitation based on observed SWE and simulated sublimation. VIC model-simulated annual sublimation is compared with the estimates of Liston and Sturm (1998) in Fig. 8c. Despite the differences in precipitation, both models produce similar estimates in total sublimation. The lower sublimation rates predicted by both models in 1990 are due primarily to lower sustained wind speeds in 1990 than in 1988 and 1989 (Liston and Sturm 1998).

b. Trail Valley Creek, Northwest Territories, Canada

Trail Valley Creek is a 68-km^2 research basin located 50 km north of Inuvik, Northwest Territories, on the Canadian Arctic coastal plain. Dominant vegetation includes sparse moss and lichen tundra in the upland regions and alder or willow shrub tundra on moister hill slopes and valley bottoms (Marsh and Pomeroy 1996; Pomeroy et al. 1997). Open water and black spruce forest make up less than 5% of the basin area. The topography is characterized by an east–west trending valley that is incised into a raised plateau, resulting in more complex topography than that of Imnavait Creek (Fig. 4a). The catchment was represented by one VIC model grid cell with four vegetation types (open water, tundra, shrub tundra, and forest) based on the major land cover classes observed to have influence on snow redistribution in the basin (Essery et al. 1999). Half-hourly observations of wind speed, relative humidity (over water), air temperature, and gauge-corrected precipitation were obtained from a meteorological station operated in the basin by the National Hydrology Research Institute, Environment Canada (Pomeroy and Li 2000). The relative humidity was converted to be with respect to ice, by multiplying by the ratio of e_s(water)/e_s(ice) (Bras 1990). Half-hourly observations were aggregated to hourly for the VIC application, which was run from September 1996 through April 1997. The terrain distribution and autocorrelation were calculated from a 40-m DEM of the area, so no fractal scaling was needed for this application. The 40-m DEM was digitized from a 1:50 000 topographic map (Pomeroy et al. 1997).

The time series of basin-averaged snow accumulation, snowfall, and cumulative sublimation simulated by the VIC model with the blowing-snow sublimation algorithm are shown in Fig. 9. Sublimation during blowing-snow events was simulated in the Trail Valley Creek watershed from 11 September 1996 through 8 April 1997 by Essery et al. (1999) using a parametric adaptation of the physically based Prairie Blowing Snow Model (Pomeroy et al. 1993), the Distributed Blowing Snow Model (DBSM). The DBSM conducts a mass balance for each grid cell and adjusts the parametrically calculated transport and sublimation fluxes using the probability of blowing-snow occurrence. Probability of occurrence is based on wind speed, snow condition, vegetation density, and vegetation exposure above the snowpack. In this case, wind speed and direction for each grid cell were calculated using the linear windflow model of Walmsley et al. (1982).

Basin-average total sublimation from blowing snow for the simulated period was 26 mm from the VIC model as compared with 73 mm estimated by Essery et al. (1999). Approximately 66% of this discrepancy is due to differences in relative humidity. Essery et al. (1999) did not adjust the observed humidity for ice saturation, resulting in lower humidity inputs on average. The SWE simulated for each vegetation class are compared with observations in Fig. 10a (black diamonds). The lakes were not sampled. The total SWE for open tundra is

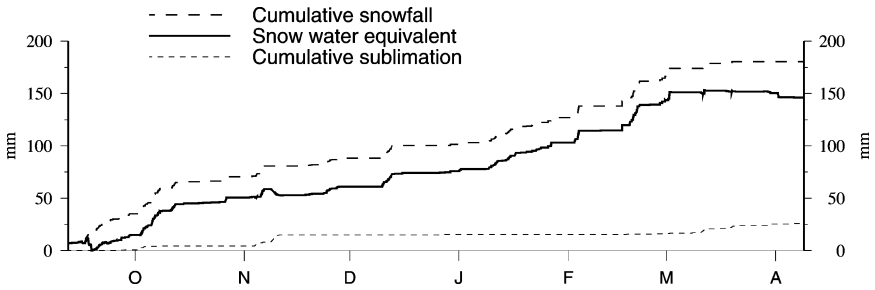

FIG. 9. Accumulated snowfall, snow water equivalent, and sublimation predicted using the VIC blowing-snow algorithm for Trail Valley Creek.

overpredicted, while total accumulation in the shrub tundra and forest are underpredicted by VIC by approximately 50 mm. Observed SWE in the forest and shrubs (215 and 219 mm, respectively) exceeds total precipitation (180 mm). This illustrates that for regions with intermixed vegetation, snow transport from one vegetation class to another, which is not represented by the VIC model, can be important to representing the spatial distribution of SWE. Essery et al. (1999) explicitly represented snow transport into the shrub and forests from the upwind lake and open tundra areas for Trail Valley Creek. Using the snow loss or gain from each vegetation type estimated by Essery et al. (1999) to adjust the VIC model-simulated SWE results in the open triangles shown in Fig. 10a. The adjustment results in an overprediction of SWE for all three vegetation classes, but with a smaller mean bias than the unadjusted SWE.

The lack of representation of snow redistribution between vegetation types may also affect the estimation of sublimation, as shown in Fig. 10b. The VIC algorithm duplicates the general trend in differences between vegetation types, but total sublimation from the shrubs and forests are lower in the VIC model simulations than in Essery et al. (1999), both with and without the relative humidity adjustment (not shown). The additional snow input into shrub and forests by transport fills vegetation roughness elements earlier in the snow season, thus increasing the calculated probability of blowing snow. This indicates that for accurate representation of subgrid variability in SWE, representation of snow transport between vegetation classes may be important.

c. Kuparuk River, Alaska

The full capabilities of the VIC model blowing-snow algorithm, including scaling of the terrain slope distribution and simplified representation of large spatial domains were employed for the ~8000-km^2 Kuparuk River basin in northern Alaska (see Fig. 1). The Kuparuk River drains north from the foothills of the Brooks Range to the Arctic Ocean. Imnavait Creek is located in the headwaters of the Kuparuk River. Moving northward from Imnavait Creek, the topography transitions to the relatively flat Arctic coastal plain, as shown in Fig. 11. Vegetation of the coastal plain consists primarily of tussock tundra and wetlands.

The Kuparuk River was simulated as 153 VIC model grid cells at ⅛° resolution. The simulation was run continuously (year round) from 1 October 1993 through 30 September 1997, with a 1-h time step. The average fetch

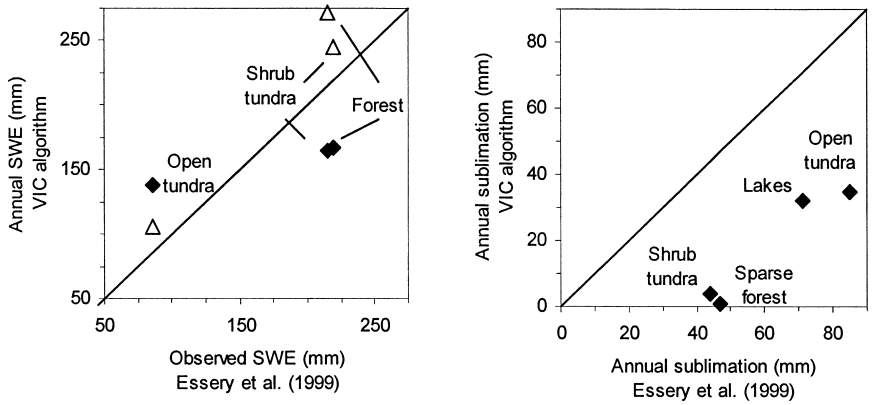

FIG. 10. Comparison of (a) annual maximum SWE observed and predicted using the VIC model. The open triangles represent VIC model-simulated SWE adjusted by the snow-transport rates between vegetation classes estimated by Essery et al. (1999). (b) Accumulated sublimation for each vegetation type for Trail Valley Creek predicted by the VIC model and by Essery et al. (1999) with the Distributed Blowing Snow Model.

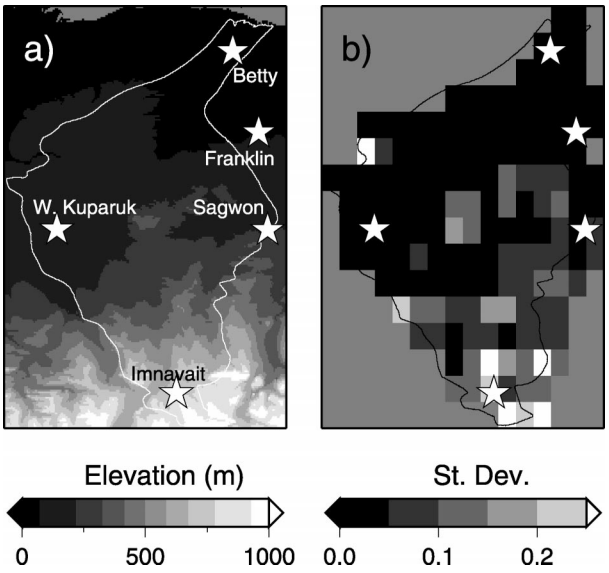

FIG. 11. Spatial variation of terrain parameters in the Kuparuk River basin: (a) 30 arc second elevations and (b) standard deviation of terrain slope.

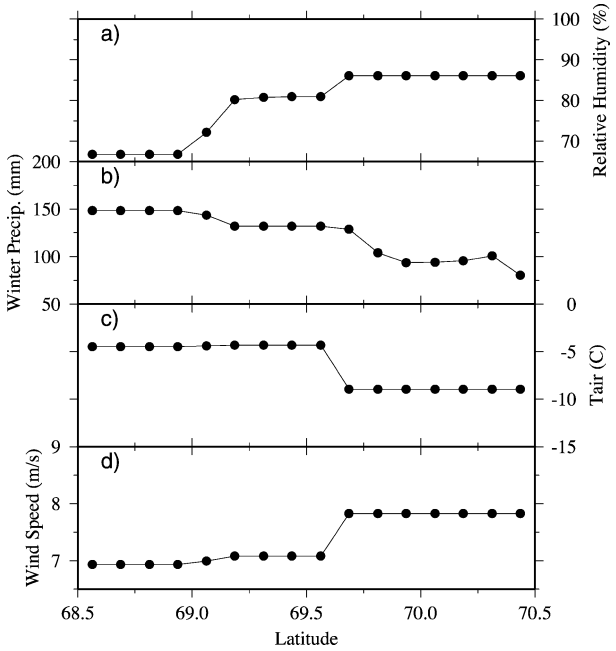

FIG. 12. Average gridded meteorological inputs for the Kuparuk River basin for the winter months (1 Sep through 30 Apr), averaged over all longitudes to create average north–south transects of (a) average relative humidity, (b) accumulated precipitation, (c) average air temperature, and (d) average wind speed. Air temperature, relative humidity, and wind speed averages were calculated only for days on which the average daily wind speed exceeded 5 m s^{-1} to approximate blowing-snow conditions.

for each grid cell was taken from the combined topography/vegetation calculation illustrated in Fig. 6c. The terrain slope variances were scaled according to Eq. (10) with θ calculated from the fractal dimension of each grid cell.

Hourly relative humidity, air temperature, and wind speed were obtained from eight meteorological stations in the basin operated by WERC (Kane and Hinzman 2003). Daily precipitation was obtained from two National Climatic Data Center (NCDC) cooperative observer stations operated near the basin (Prudhoe Bay and Kuparuk) and two Natural Resource Conservation Service (NRCS) snow telemetry sites (Imnavait Creek and Sagwon Wyoming gauges). NCDC precipitation was corrected for wind-induced gauge undercatch using a correction devised for the 8-in. standard U.S. National Weather Service gauge as part of the WMO precipitation gauge intercomparison project (Yang et al. 1998). Catch correction for the NRCS Wyoming snow gauges was performed as described for Imnavait Creek. Precipitation bias adjustment is often approximate, particularly for liquid and mixed precipitation, so the true precipitation quantity remains a large source of uncertainty. Meteorological inputs were interpolated to the resolution of the VIC model grid (⅛° latitude by longitude) using a least-distance-squared interpolation routine (the SYMAP algorithm; Shepard 1984). Observed relative humidity is multiplied by saturated vapor pressure (w.r.t. ice in this case, as discussed above) to convert to vapor pressure prior to interpolation. Internally to the model, vapor pressure is converted back to relative humidity using interpolated air temperature to estimate saturated vapor pressure with respect to ice following Shuttleworth (1993) and Bras (1990).

As shown in Fig. 12, meteorological conditions have a strong north–south gradient. Wind speeds and average relative humidity tend to increase along the exposed coastal plain, while average air temperature decreases. The corrected, gauge-measured precipitation also drops with the transition to the coastal plain.

Average modeled sublimation from blowing snow (accumulated for the winters 1994/95, 1995/96, and 1996/97, then averaged) is shown in Fig. 13 for a north–south transect of the Kuparuk River basin. Grid-cell-average sublimation was further averaged across all longitudes to create the transect. The modeled latitudinal average varies from a high of 47 mm in the foothills to a low of 10 mm in the central portion of the basin. Average simulated blowing-snow sublimation on the coastal plain (taken as north of 69.75°N) is approximately 31 mm. The area of lowest estimated blowing-snow sublimation corresponds to a transitional region between the foothills and the coastal plain, where the average wind speed reflects the lower foothills values (Fig. 12d) and the relative humidity reflects the higher coastal plain values (Fig. 12a). The spatial distribution of estimated blowing-snow sublimation as a percentage of snowfall (precipitation falling at temperatures less than zero from 1 September to 30 April) is shown in Fig. 14. From this figure it is clear that the lowest estimates of sublimation center around the West Kuparuk

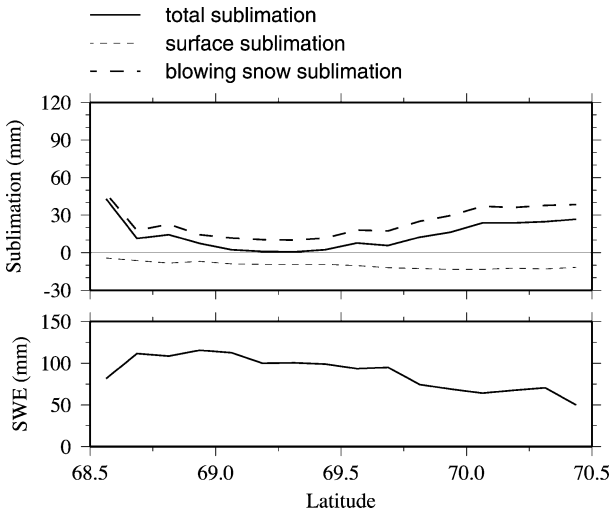

FIG. 13. Average sublimation during blowing snow, sublimation from the snowpack surface, and total sublimation (blowing sublimation plus surface sublimation) for the Kuparuk River basin. Negative sublimation implies net condensation. Sublimation was averaged over all longitudes to create an average north–south transect.

meteorological station. This station is situated in a region of less complex, coastal plain topography (see Fig. 11), which results in less variation in the parameterized spatial distribution of wind speed, and hence lower estimates of sublimation.

Figure 14 also shows a comparison of simulated and observed annual maximum SWE for 1994 through 1997 for five of the WERC meteorological station locations, both with and without the blowing-snow algorithm. There is a great deal of scatter due in part to the mismatch in scale between what are essentially point observations and grid-cell-average predictions. On average, the simulated SWE with blowing snow is closer to observations than the simulations without blowing snow, for all locations except Imnavait Creek. As discussed above, the underprediction at Imnavait Creek continues to reflect a problem with precipitation undercatch, since the corrected precipitation was still not greater than the observed SWE for one of the four years.

Liston and Sturm (2002) simulated sublimation from blowing snow using the SnowTran-3D model for an 85 km × 230 km region centered on the Kuparuk River.

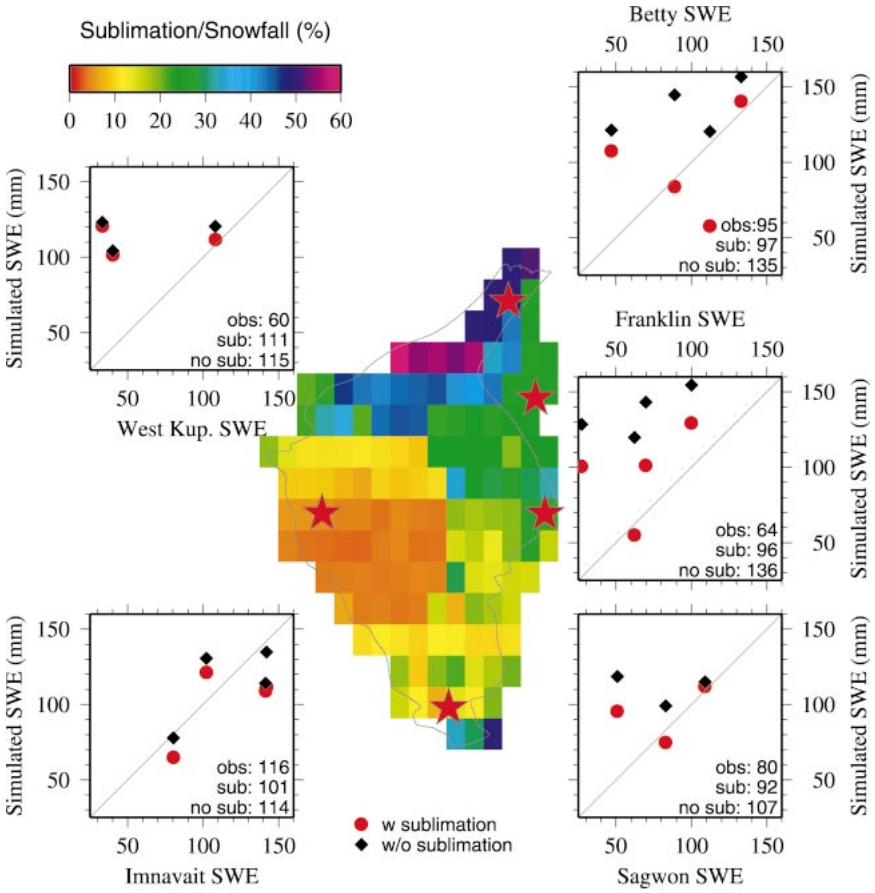

FIG. 14. Simulated blowing-snow sublimation as a percentage of snow precipitation (map) and observed vs simulated SWE for five WERC observation locations (scatterplots). Red dots indicate VIC model simulations with blowing snow and black dots indicate simulations without the blowing-snow algorithm.

Their application utilized a 100 m × 100 m horizontal grid, and daily time step and simulations were performed for the winters of 1994/95 to 1996/97. Both the VIC model and SnowTran-3D estimate a region of low sublimation in the central portion of the basin, with increasing sublimation toward the foothills and coastal plain (see Fig. 13). In 1995, blowing-snow sublimation predicted by Liston and Sturm along an average transect varies from approximately 20 to 40 mm in the uplands, transitions to approximately 20 mm in the central region, and then increases to a high of 100 mm on the coastal plain. The VIC model predictions for 1995 (not shown) vary from 20 to 50 mm in the uplands, to a low of 15 mm, increasing to 80 mm on the coastal plain. As a percentage of snow precipitation, VIC model estimates of blowing-snow sublimation averaged over all years range from 10% to 37% in the foothills to 30% to 50% on the coastal plain (see Fig. 14). These are roughly similar to those of Liston and Sturm (2002), which vary from 10% to 20% in the foothills and 20% to 45% on the coastal plain. Figure 14 shows greater east–west variation in sublimation than Liston and Sturm (2002). They assumed a uniform east–west profile in meteorological forcings, in contrast to the spatially explicit interpolation performed here.

As described above, precipitation input for the VIC application was obtained by gridding catch-corrected station observations. Liston and Sturm (2002) used extensive snow surveys to determine the end-of-winter distribution of SWE in April of 1995, 1996, and 1997. They then used an iterative process with the blowing-snow model to estimate the precipitation inputs necessary to provide a best fit to an observed north–south transect of SWE. Such a procedure optimizes the precipitation input to calibrate the SWE prediction of a specific model to observations; the suitability of precipitation estimated in this manner for other purposes cannot be fully evaluated. The assimilation method of Liston and Sturm (2002) yielded estimates of annual average precipitation approximately 50 to 60 mm greater than the corrected gauge data throughout the model domain. The trend in precipitation for the upland-coastal plain transition and the coastal plain is similar between the two methods.

Blowing-snow sublimation is tied to both the timing and quantity of precipitation. Transport of snow by wind cannot be initiated in SnowTran-3D until the snow-holding capacity of vegetation is satisfied. The calculation is different in the VIC model, but exposed vegetation also has a strong effect in suppressing blowing snow. In addition, increasing time since the last snowfall decreases the probability of occurrence of blowing snow, as parameterized in the VIC model using the formulation of Li and Pomeroy (1997). Underestimation of the magnitude or frequency of precipitation events (i.e., from unrecorded trace events), will therefore result in a lower estimate of blowing-snow sublimation.

Direct observations of sublimation in the subarctic and Arctic are rare; however, Harazono et al. (2002) observed sublimation during a 2-day blowing-snow event on the Arctic coastal plain near Barrow, Alaska, on the order of 6.4 mm. Total sublimation from October 2000 through March 2001 was observed to be 13.5 mm (Harazono et al. 2003). Simulated blowing-snow sublimation for the grid cell corresponding to the Betty site, which should be similar to the Barrow location, varied between 13 and 89 mm for October through March 1994 through 1997. Point observations of SWE are also fairly well represented at the Betty site (Fig. 14), further suggesting the feasibility of the VIC model estimates of blowing-snow sublimation on the coastal plain. The SWE observations of Liston and Sturm (2002) are heavily weighted toward the uplands, and Liston and Sturm (2002) acknowledge that their simulations near the coast likely have the largest errors. In the uplands, SWE is underpredicted by the VIC model both in the point comparisons at Imnavait Creek and in comparison with the observed transect of Liston and Sturm (2002). Estimates of blowing sublimation in the uplands is similar between the VIC model and Liston and Sturm (2002), suggesting that the underprediction of SWE by the VIC model is due to underprediction of precipitation inputs.

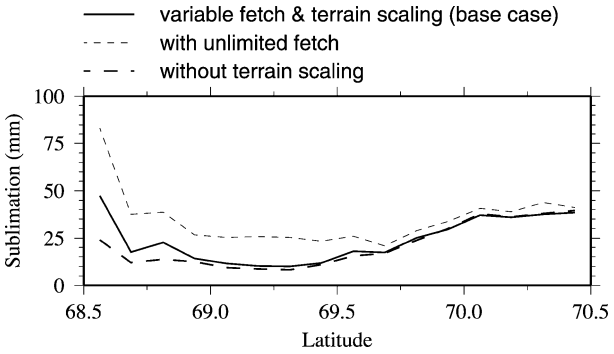

FIG. 15. Comparison of average sublimation from blowing snow computed with the VIC model for three blowing-snow algorithm parameterizations: (1) with spatially varying fetch and fractal scaling of terain slopes, (2) without spatially varying fetch (unlimited fetch), and (3) without fractal scaling of terrain slopes.

4. Discussion and sensitivity

The representation of subgrid variability in terrain and fetch in the VIC model blowing-snow algorithm and the influence of the snow surface energy balance result in both increases and decreases in total snow sublimation fluxes compared to those that would be predicted by a stand-alone column model. The influence of the VIC model parameterizations on estimated blowing-snow sublimation rates is shown in Fig. 15. A simulation with no fetch limitation results in an 85% increase in sublimation rates in the foothills where the complex terrain creates areas of limited fetch. The difference is much smaller on the coastal plain (11%), where the calculated

average fetch is sufficiently large (1 to 2 km) that it does not impose a significant limitation on sublimation rates.

The effect of the rescaling of the terrain distribution on the simulated blowing-snow sublimation is also shown in Fig. 15. Using the variance in terrain slope calculated directly from the 30 arc second DEM results in 60% less sublimation in the foothills and 1% less on the coastal plain. The larger effect in the foothills is expected, as the complex topography of the foothills results in a greater spread of the spatial wind distribution. This is reflected in the standard deviation of terrain gradient shown in Fig. 11b. The relationship of sublimation to wind speed is extremely nonlinear (King et al. 2001; Essery et al. 1999; Mikhel and Rudneva 1967), so greater spread in the distribution results in a higher mean sublimation. The insensitivity of sublimation to the wind parameterization on the coastal plain is evidence that blowing-snow sublimation in this region is limited by snow availability for transport, rather than transport capacity; a higher snowfall input would increase the sensitivity in this region.

Surface sublimation from the snow pack and total sublimation (blowing-snow sublimation plus surface sublimation) are also shown in Fig. 13. For the entire average transect, the simulated seasonal surface sublimation results in net condensation (although not for every grid cell). Liston and Sturm (2002) do not simulate vapor exchange with the snowpack. Net seasonal condensation is not anticipated from observations reported in the literature; however, continuous overwinter observations of vapor flux in arctic environments are extremely difficult and rare, so the validity of these estimates can also not be disproven. Simulated surface sublimation in the VIC model is driven by the vapor pressure gradient between the atmosphere and the snow surface, with a correction for atmospheric stability. Snow surface vapor pressure is assumed to equal saturation vapor pressure with respect to ice at the snow surface temperature. Snow surface temperature is solved by iteration in order to close the surface energy balance. In midwinter, low snow surface temperatures result in a negative vapor pressure gradient even at times when the atmospheric relative humidity is less than 100%. The latent heat consumed by blowing-snow sublimation further reduces the snow surface temperature, so surface condensation is slightly higher for the VIC model runs with blowing snow than those without (not shown). In contrast, as derived by Thorpe and Mason (1966), sublimation from a suspended ice particle is independent of the temperature of the particle surface; it is dependent only on the atmospheric humidity. Therefore, sublimation from suspended snow particles can be maintained at times when surface sublimation cannot.

There are a couple of factors that may contribute to a possible overprediction of surface condensation by the VIC model. Pomeroy et al. (1998) compared the predictions of three turbulent transfer schemes commonly used in land surface schemes with observations near Saskatoon, Saskatchewan, Canada, for a 2-day period in March 1996. They found that the downward turbulent energies were overestimated by all three models. Although not tested for the VIC model, the rate of condensation predicted for the Kuparuk basin may be due in part to inadequate dampening of turbulent mixing during stable conditions.

In addition, the atmospheric water vapor pressure for this application is calculated from station observations of relative humidity. Humidity measurements in arctic environments are frequently overestimated because of ice accumulation on the gauge. Déry and Stieglitz (2002) recently documented the tendency of the Vaisala hygrothermomenters to overpredict vapor saturation. In addition, it is frequently unclear whether such instruments measure relative humidity for water vapor in equilibrium with a liquid or frozen surface. For the reasons described above, the simulated surface sublimation is sensitive to small absolute changes in winter vapor pressure. Uncertainty in the measured relative humidity is undoubtedly influential in the estimates of net surface condensation in this region.

5. Conclusions

This study develops a framework for predicting blowing-snow sublimation within the Variable Infiltration Capacity (VIC) macroscale hydrology model, including an approximation of topographically induced subgrid variability in wind speed. VIC model-predicted SWE compares favorably to observed SWE in several locations. In addition, predicted blowing-snow sublimation from the VIC model is consistent with estimates from two different high-resolution blowing-snow algorithms (Liston and Sturm 1998; Essery et al. 1999) and with limited observations at Barrow, Alaska. In general, the comparisons indicate that the VIC algorithm results in feasible estimates of sublimation and reproduced most aspects of the variability between years predicted by the other models. Comparison of the VIC model results with the distributed model results allows assessment of the ability of the VIC blowing-snow algorithm to parameterize subgrid variability in wind speed and fetch.

Complete validation of the model is complicated by both the difference in scale between model predictions (⅛° latitude by longitude) and observations and by problems in accurate measurement of the pertinent variables. The midwinter snow balance in arctic landscapes can be approximated as SWE = snow precipitation − sublimation. Direct measurements of sublimation are difficult (Pomeroy and Essery 1999), and precipitation measurements are highly unreliable because of precipitation gauge undercatch (Goodison et al. 1998; Pomeroy and Goodison 1997). In addition, estimates of sublimation are very sensitive to relative humidity, which are frequently overestimated because of ice accumulation on the gauges (Déry and Stieglitz 2002). Innovative

measurement techniques for extreme environments are essential for resolving the uncertainty in similar studies.

The VIC model was subsequently used to estimate sublimation and SWE for the 8000-km^2 Kuparuk River watershed in northern Alaska. Based on these model simulations, and point simulations at Imnavait Creek, Alaska, and Trail Valley Creek, Northwest Territories:

- Subgrid variability in wind speed exerts a strong control on blowing-snow transport and sublimation at the mesoscale.
- Annual average blowing-snow sublimation for individual grid cells varies from 4 to 63 mm in the Kuparuk River basin on the Alaskan North Slope. A regional low in blowing-snow sublimation occurs along the transition from the foothills to the coastal plain due to lower wind speeds, higher relative humidity, and relatively flat terrain.
- The simulated blowing-snow sublimation is sensitive to estimates of upwind fetch in regions of complex terrain. Blowing-snow sublimation is primarily limited by fetch in the foothills and by vapor pressure and precipitation on the coastal plain.
- Gauge undercatch, even after precipitation is catch corrected, is a likely cause of underprediction of SWE in the foothills. Blowing-snow sublimation is tied to both the timing and quantity of precipitation and may also be underpredicted as a result.
- Vapor flux to the snowpack results in net condensation for the winter between 1 and 15 mm for individual grid cells throughout the basin. The combined fluxes therefore yield an estimate of total sublimation over the winter between 6 and 56 mm. The cause and validity of the estimated condensation requires further analysis.
- Transport of snow between vegetation classes, which is not represented by the VIC algorithm, is a process that may prove important for estimation of subgrid variability in SWE. In areas of contrasting vegetation, neglecting transport may result in an underprediction of grid-cell-average sublimation by delaying the initiation of sublimation from the trapping vegetation.

Acknowledgments. Funding for this project was provided by a NASA Earth System Science fellowship to the first author, and by NASA Grant NAGS-11632 and National Science Foundation Award 0230327 to the University of Washington. Meteorologic and snow water equivalent data at Trail Valley Creek were collected with funding from the Canadian Mackenzie GEWEX Study (MAGS) through grants from Environment Canada and the Natural Sciences and Engineering Research Council of Canada. Meteorologic and snow water equivalent data for Imnavait Creek and the Kuparuk River basin were collected by the University of Alaska Fairbanks (UAF), Water and Environmental Research Center (WERC) North Slope Hydrology Research Project and provided digitally through the National Snow and Ice Data Center. Thanks also to Rob Gieck, of UAF, for providing additional details regarding this data. Richard Essery and Glen Liston shared both electronic data and insight related to their research and modeling, which is greatly appreciated. This manuscript was improved by the comments of Stephen Déry, Glen Liston, and one anonymous reviewer.

REFERENCES

Benson, C. S., 1982: Reassessment of winter precipitation on Alaska's Arctic slope and measurements on the flux of wind-blown snow. Geophysical Institute Rep. UAG R-288, Geophysical Institute, University of Alaska, Fairbanks, 26 pp.

Berg, N. H., 1986: Blowing snow at a Colorado alpine site: Measurements and implications. *Arct. Alp. Res.*, **18,** 147–161.

Bintanja, R., 1998: The contribution of snowdrift sublimation to the surface mass balance of Antarctica. *Ann. Glaciol.*, **27,** 251–259.

——, 2001: Modelling snowdrift sublimation and its effects on the moisture budget of the atmospheric boundary layer. *Tellus*, **53A,** 215–232.

Bras, R. L., 1990: *Hydrology: An Introduction to Hydrologic Science.* Addison-Wesley, 643 pp.

Cherkauer, K. A., and D. P. Lettenmaier, 1999: Hydrologic effects of frozen soils in the upper Mississippi River basin. *J. Geophys. Res.*, **104** (D16), 19 599–19 610.

——, L. C. Bowling, and D. P. Lettenmaier, 2003: Variable Infiltration Capacity (VIC) Cold Land Process Model updates. *Global Planet. Change*, **38,** 151–159.

Déry, S. J., and M. K. Yau, 1999: A Climatology of adverse winter-type weather events. *J. Geophys. Res.*, **104** (D14), 16 657–16 672.

——, and ——, 2001: Simulation of blowing snow in the Canadian Arctic using a double-moment model. *Bound.-Layer Meteor.*, **99,** 297–316.

——, and M. Stieglitz, 2002: A note on surface humidity measurements in the cold Canadian environment. *Bound.-Layer Meteor.*, **102,** 491–497.

——, P. A. Taylor, and J. Xiao, 1998: The thermodynamic effects of sublimating, blowing snow in the atmospheric boundary layer. *Bound.-Layer Meteor.*, **89,** 251–283.

Dyunnin, A. K., 1959: Fundamentals of the theory of snowdrifting. *Izv. Sib. Otd. Akad. Nauk SSSR*, **12,** 11–24. (Translated from Russian by G. Belkov.)

Essery, R., 2001: Spatial statistics of windflow and blowing-snow fluxes over complex topography. *Bound.-Layer Meteor.*, **100,** 131–147.

——, L. Li, and J. Pomeroy, 1999: A distributed model of blowing snow over complex terrain. *Hydrol. Processes*, **13,** 2423–2438.

Goodison, B. E., P. Y. T. Louie, and D. Yang, 1998: WMO solid precipitation measurement intercomparison: Final report. World Meteorological Organization Tech. Doc. WMO/TD-872, 212 pp.

Groisman, P. Y., V. S. Golubev, E. L. Genikhovich, and S. Bomin, 1997: Evaporation from snow cover: An empirical study. *Proc. Conf. on Polar Processes and Global Climate*, Rosario, WA, ACSYS, 72–73.

Gupta, V. K., and E. Waymire, 1990: Multiscaling properties of spatial rainfall and river flow distributions. *J. Geophys. Res.*, **95** (D3), 1999–2009.

Harazono, Y., M. Mano, H. Kitauchi, A. Miyata, and W. C. Oechel, 2002: Winter fluxes of CO_2 and energy at tundra in the Arctic. *Eos, Trans. Amer. Geophys. Union*, **83** (Fall Meeting Suppl.), Abstract GC72B-0235.

——, W. C. Oechel, A. Miyata, and M. Mano, cited 2003: Direct observation of winter sublimation and its effects on the arctic climate. *Abstracts, SEARCH Open Science Meeting*, Seattle, WA, NSF Office of Polar Programs. [Available online at http://www.arcus.org/search/OSM/abstracts.shtml.]

Hinzman, L. D., D. L. Kane, C. S. Benson, and K. R. Everett, 1996:

Energy balance and hydrological processes in an Arctic watershed. *Ecol. Stud.,* **120,** 131–154.
Hood, E. W., M. W. Williams, and D. Cline, 1998: Sublimation from a seasonal snowpack at a continental, mid-latitude alpine site. *Hydrol. Processes,* **13,** 1781–1797.
Kane, D. L., and L. D. Hinzman, cited 2003: Meteorological and hydrographic data, Kuparuk River Watershed, National Snow and Ice Data Center, Boulder, CO. [Available online at http://www.nsidc.org/data/arcss015.html.]
——, ——, C. S. Benson, and G. E. Liston, 1991: Snow hydrology of a headwater Arctic basin: I. Physical measurements and process studies. *Water Resour. Res.,* **27,** 1099–1109.
——, ——, J. P. McNamara, Z. Zhang, and C. S. Benson, 2000: An overview of a nested watershed study in Arctic Alaska. *Nord. Hydrol.,* **31,** 245–266.
Kind, R. J., 1992: One-dimensional aeolian suspension above beds of loose particles—A new concentration-profile equation. *Atmos. Environ.,* **26A,** 927–931.
King, J. C., P. S. Anderson, and G. W. Mann, 2001: The seasonal cycle of sublimation at Halley, Antarctica. *J. Glaciol.,* **47,** 1–8.
Klinkenberg, B., and M. F. Goodchild, 1992: The fractal properties of topography: A comparison of methods. *Earth Surf. Processes Landforms,* **17,** 217–234.
Kono, N., 1985: Hausdorff dimension of sample paths for self-similar processes. *Dependence in Probability and Statistics,* E. Berlein and M. Taqqu, Eds., Birkhauser, 109–118.
Lavalée, D., S. Lovejoy, D. Schertzer, and P. Ladoy, 1993: Nonlinear variability of landscape topography. *Multifractal Analysis and Simulation,* N. Lam and L. DeCola, Eds., Prentice-Hall, 171–205.
Li, L., and J. W. Pomeroy, 1997: Probability of occurrence of blowing snow. *J. Geophys. Res.,* **102** (D18), 21 955–21 964.
Liang, X., D. P. Lettenmaier, E. F. Wood, and S. J. Burges, 1994: A simple hydrologically based model of land surface water and energy fluxes for general circulation models. *J. Geophys. Res.,* **99** (D7), 14 415–14 428.
Liston, G., and M. Sturm, 1998: A snow-transport model for complex terrain. *J. Glaciol.,* **44,** 498–516.
——, and ——, 2002: Winter precipitation patterns in Arctic Alaska determined from a blowing-snow model and snow-depth observations. *J. Hydrometeor.,* **3,** 646–659.
Lovejoy, S., D. Lavallee, D. Schertzer, and P. Ladoy, 1995: The $1^{1/2}$ law and multifractal topography: Theory and analysis. *Nonlinear Processes Geophys.,* **2,** 16–22.
Mann, G. W., P. S. Anderson, and S. D. Mobbs, 2000: Profile measurements of blowing snow at Halley, Antarctica. *J. Geophys. Res.,* **105** (D19), 24 491–24 508.
Marsh, P., and J. W. Pomeroy, 1996: Meltwater fluxes at an Arctic forest–tundra site. *Hydrol. Processes,* **10,** 1383–1400.
Maurer, E. P., A. W. Wood, J. C. Adam, D. P. Lettenmaier, and B. Nijssen, 2002: A long-term hydrologically based dataset of land surface fluxes and states for the conterminous United States. *J. Climate,* **15,** 3237–3251.
Mikhel, V. M., and A. V. Rudneva, 1967: Regionalization of the USSR according to the transport of snow. *Sov. Hydrol.,* **5,** 441–449.
Muller, S. V., A. E. Racoviteanu, and D. A. Walker, 1999: Landsat-MSS-derived land-cover map of northern Alaska: Extrapolation methods and comparison with photo-interpreted and AVHRR-derived maps. *Int. J. Remote Sens.,* **20,** 2921–2946.
Nijssen, B., R. Schnur, and D. Lettenmaier, 2001: Global retrospective estimation of soil moisture using the variable infiltration capacity land surface model, 1980–1993. *J. Climate,* **14,** 1790–1808.
Petropavlovskaya, M. S., and I. L. Kalyuzhnyi, 1986: Drifting of snow in Northern Kazakhstan. *Sov. Meteor. Hydrol.,* **2,** 67–74.
Pomeroy, J. W., 1989: A process-based model of snow drifting. *Ann. Glaciol.,* **13,** 237–240.
——, and D. M. Gray, 1990: Saltation of snow. *Water Resour. Res.,* **26,** 1583–1594.
——, and D. H. Male, 1992: Steady-state suspension of snow. *J. Hydrol.,* **136,** 275–301.
——, and D. M. Gray, 1995: Snowcover accumulation, relocation and management. National Hydrology Research Institute Science Rep. 7, Environment Canada, Saskatoon, SK, Canada, 144 pp.
——, and B. E. Goodison, 1997: Winter and snow. *The Surface Climates of Canada,* W. G. Bailey, T. R. Oke, and W. R. Rouse, Eds., McGill-Queen's University Press, 68–100.
——, and R. L. H. Essery, 1999: Turbulent fluxes during blowing snow: Field tests of model sublimation predictions. *Hydrol. Processes,* **13,** 2963–2975.
——, and L. Li, 2000: Prairie and arctic areal snow cover mass balance using a blowing snow model. *J. Geophys. Res.,* **105** (D21), 26 629–26 634.
——, D. M. Gray, and P. G. Landine, 1993: The Prairie Blowing Snow Model: Characteristics, validation, operation. *J. Hydrol.,* **144,** 165–192.
——, P. Marsh, and D. M. Gray, 1997: Application of a distributed blowing snow model to the Arctic. *Hydrol. Processes,* **11,** 1451–1464.
——, D. M. Gray, K. R. Shook, B. Toth, R. L. H. Essery, A. Pietroniro, and N. Hedstrom, 1998: An evaluation of snow accumulation and ablation processes for land surface modeling. *Hydrol. Processes,* **12,** 2339–2367.
Schmidt, R. A., 1972: Sublimation of wind-transported snow—A model. USDA Res. Paper RM-90, USDA Forestry Service, Rocky Mountain Forest and Range Experimental Station, Fort Collins, CO, 24 pp.
——, 1982: Vertical profiles of wind speed, snow concentration, and humidity in blowing snow. *Bound.-Layer Meteor.,* **23,** 223–246.
Shepard, D. S., 1984: Computer mapping: The SYMAP interpolation algorithm. *Spatial Statistics and Models,* G. L. Gaile and C. J. Willmott, Eds., Reidel, 133–145.
Shuttleworth, W. J., 1993: Evaporation. *Handbook of Hydrology,* D. R. Maidment, Ed., McGraw-Hill, 4.1–4.53.
Tabler, R. D., 1975a: Estimating the transport and evaporation of blowing snow. *Proc. Symp. on Snow Management on the Great Plains,* Bismarck, ND, Great Plains Agricultural Council, Publication 73, 85–104.
——, 1975b: Predicting profiles of snowdrifts in topographic catchments. *Proc. 43rd Western Snow Conf.,* Coronado, CA, Western Snow Conference, 87–97.
Takeuchi, M., 1980: Vertical profile and horizontal increase of drift-snow transport. *J. Glaciol.,* **26,** 481–492.
Thorpe, A. D., and B. J. Mason, 1966: The evaporation of ice spheres and ice crystals. *Br. J. Appl. Phys.,* **17,** 541–548.
van den Broeke, M. R., J. G. Winther, E. Isaksson, J. F. Pinglot, L. Karlof, T. Eiken, and L. Conrads, 1999: Climate variables along a traverse line in Dronning Maud Land, East Antarctica. *J. Glaciol.,* **45,** 295–302.
Walker, D. A., cited 1996: GIS data from the Alaska North Slope. National Snow and Ice Data Center. [Available online at http://www.nsidc.org/data/arcss017.html.]
Walmsley, J. L., J. R. Salmon, and P. A. Taylor, 1982: On the application of a model of boundary-layer flow over low hills to real terrain. *Bound.-Layer Meteor.,* **23,** 17–46.
Xiao, J., R. Bintanja, S. Déry, G. Mann, and P. Taylor, 2000: An intercomparison among four models of blowing snow. *Bound.-Layer Meteor.,* **97,** 109–135.
Xu, T., I. D. Moore, and J. C. Gallant, 1993: Fractals, fractal dimensions and landscapes—A review. *Geomorphology,* **8,** 245–262.
Yang, D., B. E. Goodison, and S. Ishida, 1998: Adjustment of daily precipitation data at 10 climate stations in Alaska: Application of World Meteorological Organization intercomparison results. *Water Resour. Res.,* **34,** 241–256.
——, and Coauthors, 2000: An evaluation of the Wyoming gauge system for snowfall measurement. *Water Resour. Res.,* **36,** 2665–2677.
Zhang, X., N. A. Drake, J. Wainwright, and M. Mulligan, 1999: Comparison of slope estimates from low resolution DEMS: Scaling issues and a fractal method for their solution. *Earth Surf. Processes Landforms,* **24,** 763–779.